Iranian Journal of Materials Science and Engineering, Vol. 20, Number 2, June 2023
RESEARCH PAPER

Effect of Poly (3-Hexylthiophene): Mixed Fullerene Indene-C_{60} Multi-Adducts Ratios on the Performance of Organic Solar Cells

Hassan Tarikhum B.[1,2], Basil Ali[1], Furqan Almyahi[1,*], Mazin A. Mahdi[1]

* *furqan.kasim@uobasrah.edu.iq*

[1] Department of Physics, College of Science, University of Basrah, Basrah, Iraq
[2] Department of Physics, College of Science, University Al Muthanna, Al Samawa, Iraq

Received: February 2023 Revised: April 2023 Accepted: May 2023
DOI: 10.22068/ijmse.3147

Abstract: *In this study, poly (3-hexylthiophene) (P3HT) and fullerene Indene-C_{60} multi-adducts (ICxA) were blended to create a formulation as a solution and thin films, which were prepared under ambient conditions. The optical properties of various compositional ratios were studied using UV-Visible absorbance and photoluminescence (PL) measurements. The energy gaps of the prepared thin films and solutions were determined, and their values increased with increasing fullerene ratio because of the isolation of P3HT chains from their neighbors. Intensity ratio ($I_{C=C}/I_{C-C}$) with a small value in addition to a low value of full width at high maximum (FWHM) of Raman spectra are associated with increased conformation and high aggregation of composition. Furthermore, according to X-ray diffraction (XRD) results the 1:0.8 and 1:0.6 ratios have the largest crystallite sizes in comparison to the other ratios. The highest occupied molecular orbital (HOMO) and the lowest unoccupied molecular orbital (LUMO) levels for blends by electrochemical measurements were determined, which are sandwiched between those of the pure materials. In ambient conditions, binary organic photovoltaic cells (OPVs) at different ratios of the photoactive layer were evaluated. The device with a ratio of 1:0.6 had the best performance, with power conversion efficiency (PCE) of 1.21%, open circuit voltage (V_{OC}) of 0.53 V, short circuit current density (J_{SC}) of 5.71 mA.cm^{-2}, and fill factor (FF) of 39.5% at a small V_{loss} of 1.39 V.*

Keywords: *Organic photovoltaics, Photoluminescence, X-ray diffraction, Raman spectrum, Cyclic Voltammetry.*

1. INTRODUCTION

Organic materials have contributed to the development of organic photovoltaic cells (OPVs) as a new source of clean and cheap energy and have opened the way to progress in understanding the fundamental chemistry and physics of π-bonded macromolecules [1]. The OPV devices can absorb sunlight and convert it into electricity because of their conjugated system [2]. The first OPV device was constructed by Calvin in 1958 [3] using magnesium phthalocyanines (MgPc) between two conducting glass electrodes, which achieved 200 mV. The photovoltaic properties of these cells depend strongly on the nature of the electrodes. These cells are called single-layer organic photovoltaic cells and are the simplest among various organic photovoltaic cells. The first organic photovoltaic cell bilayer was reported by Tang in 1986 [4]. In these devices, light is usually absorbed in the donor material (copper phthalocyanine) and the photogenerated excitons diffuse within the donor towards the planar interface to the acceptor material (perylene tetracarboxylic derivative). A power conversion efficiency of approximately 1% has been achieved under simulated AM2 illumination (light intensity of 75 mW/cm^2). However, the performance of these devices is limited by the small interfacial area between the donor and acceptor materials, which results in impaired charge separation. To achieve high-performance OPV devices and to increase exciton dissociation in the donor/acceptor interfaces, an interpenetrated bulk heterojunction (BHJ) structure of the donor and acceptor should be achieved, which invented by Heeger et al. [5]. Blending an electron-donating conjugated polymer such as poly (3-hexylthiophene) (P3HT) with a fullerene electron acceptor such as [6, 6]-phenyl C_{60} butyric acid methyl ester (PCBM) contributed to improving the morphology of the active layer, charge separation at the donor/acceptor interface, and transport between layers of solar cells [6]. PCBM was replaced by another fullerene derivative, indene-C_{60} mono-adduct (ICBA), which has a higher LUMO than PCBM [7]. Indene: fullerene synthesized by the simple reflux of indene and fullerene, such as indene-C_{60} mono-adduct (ICMA), indene-C_{60} bis-adduct (ICBA), and indene-C_{60} tris-adduct (ICTA), which is characterized by a lower cost

[Downloaded from nezarat.iust.ac.ir on 2025-07-18]
[DOI: 10.22068/ijmse.3147]

compared to PCBM and high solubility in solvents, especially in chlorobenzene (CB). Recently, P3HT was mixed with an indene-C_{60} adduct mixture (ICxA), where x= mono-, bis-, or tris-adducts to produce roll-to-roll (R2R) OPV devices [8]. In 2010, Youjun et al. [9] synthesized a new soluble C_{60} derivative, indene-C_{60} bis-adduct (ICBA), with a LUMO energy level of 0.17 eV higher than that of PCBM. Under the same experimental conditions, the performance of OPVs using ICBA was better than that of those using PCBM. In addition, they reported that ICBA is easier to synthesize than PCBM, and it possesses better solubility in common organic solvents and stronger visible absorption than PCBM. Zhao et al. [10] studied the effect of thermal annealing on the photovoltaic performance of the P3HT: ICBA active layer. The results without thermal treatment were a PCE of 4.84%, while by annealing the active layer at 150°C for 10 min, the OPV demonstrated the best performance of PCE of 6.48%. In 2016 Cooling, et al. [11] the synthesized fullerene mixture, ICxA, was used to fabricate R2R OPV devices with the structure ITO/PEDOT:PSS/P3HT:ICxANP/Ca/Al, the results of hero type were V_{OC} of 0.81 V, J_{SC} of 7.18 mA/cm^2, FF of 58%, and PCE of 3.37%.

The present study examined the effect of the fullerene ratio on the performance of P3HT: ICxA blends by measuring steady-state spectra, structural properties, and cyclic voltammetry (CV). Scientific comparisons of the spectra of the solutions and films were performed. Raman spectroscopy was used to identify the various stretching modes present in the P3HT:ICxA thin films and the crystal structure of the blends was investigated using X–ray diffraction. The J–V properties of standard solar cells based on a binary active layer with different ratios of the P3HT:ICxA blend were also studied.

2. EXPERIMENTAL PROCEDURES

2.1. Materials

P3HT and ICxA were synthesized in-house according to the literature [11]. The ICxA consists of a mixture of 36% ICMA, 51% ICBA, and 13% ICTA. The PEDOT: PSS solution (Al 4038) low conductivity (500–5000 Ω.cm) was purchased from Ossila, UK. The ZnO nanoparticles used in this study were synthesized according to the literature [12], and the ZnO nanoparticles have a particle size of 20 nm. ITO-coated glasses for the OPV devices were purchased from South China Science and Technology Company Limited (China). These substrates were pre-coated by the manufacturer with a transparent ITO layer (thickness of approximately 100 nm and surface resistance of (8–12 Ω) in a specific pattern, which acted as the anode. Aluminum (Al) wire was commercially available, which was used as a cathode electrode, while chlorobenzene solvent (CB) was obtained from Sigma Aldrich.

2.2. Device manufacture

The P3HT: ICxA blends were prepared by dissolving 40 mg of P3HT and ICxA in 1 mL CB, at weight ratios of 1:0.6, 1:0.8, 1:1, 0.8:1, and 0.6:1.The solutions were heated at 60°C and stirred for two hours to completely dissolve materials in the solvent [13]. To characterize the physical properties, dilute solutions were prepared, as well as, thin films were made of the same prepared solutions with a spin-coating speed of 2000 rpm for 60 s [14]. Dilute solutions were prepared by adding 1 µL of P3HT: ICxA with 40 mg/mL to 4 mL of CB solvent. The thin films with an average thickness of approximately 125 nm were spin-coated on the surface of the quartz substrates (1 cm × 2 cm). To achieve a well-ordered morphology, thin films were annealed at 140°C for 5 minutes [15, 16]. To manufacture organic solar cells, the following procedures were followed: Firstly, the ITO-coated glass substrates were washed with detergent and ultrasonically cleaned in distilled water, acetone, and isopropyl alcohol. Then the substrates were dried at 100°C for 15 min in an oven. Secondly, the PEDOT: PSS layer was spin-coated on the cleaned ITO substrates at 4000 rpm for 1 min, then dried for 20 min at 140°C in air. Thirdly, on the top of PEDOT: PSS layer, the photoactive layer at 2000 rpm for 1 min was spin-coated. Fourthly, the ZnO nanoparticles layer was spin-coated on top of the photoactive layer at 4000 rpm for 1 min. After that, the annealing process was applied to the devices at 140°C for 5 min. Finally, an Al electrode was thermally deposited on top of the ZnO layer. All these procedures were performed in the air, which is shown in a schematic diagram in Figure 1, where Figure 1a represents the manufacturing steps and Figure 1b represents the structure of the OPV devices.

[Downloaded from nezarat.iust.ac.ir on 2025-07-18]

[DOI: 10.22068/ijmse.3147]

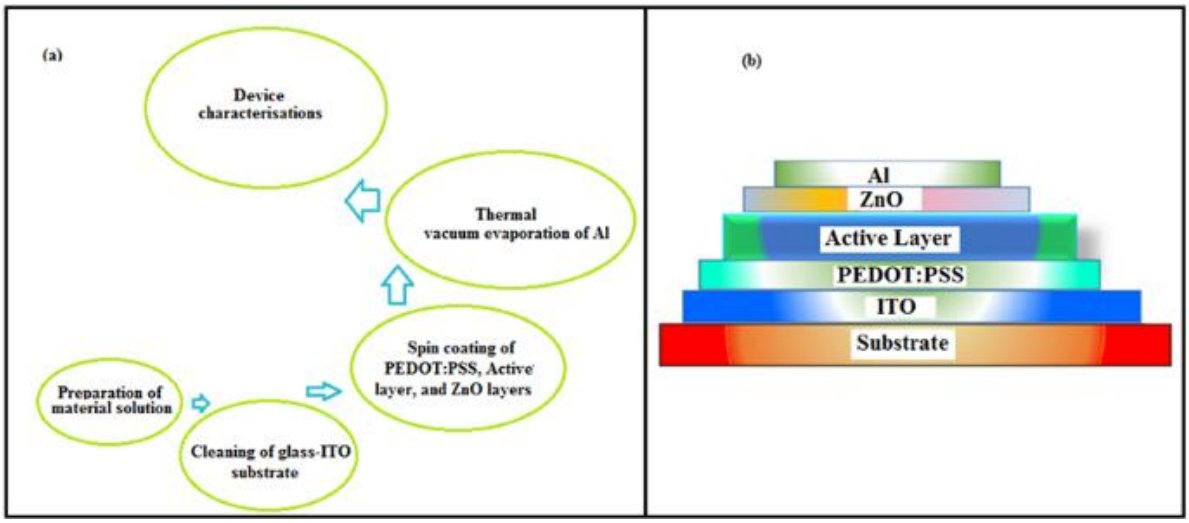

Fig. 1. A schematic diagram representing (a) the manufacturing steps and (b) the structure of the OPV devices designed according to the experimental procedure.

2.3. Characterization Techniques

Various characterization techniques were used to measure the dilute solutions and annealed thin films under ambient conditions. The absorption spectra of the samples were recorded using a Shimadzu UV-1800PC spectrometer in the range of (300–800 nm) for the dilute solutions and (200–800 nm) for the thin films. While the emission measurements were performed using a Fluo Time 300 fluorescence lifetime spectrometer at an exciting wavelength of 500 nm. On the other hand, Raman spectra were measured using a JD-785-300 mW laser with a wavelength of 532 nm, whilst, X-ray diffraction was performed using an X'Pert Diffractometer with angles ranging from 2° to 40°. The electrochemical characteristics of the thin films were investigated using the cyclic voltammetry (CV) technique. Which was carried out using a Corr-Test electrochemical workstation. The electrochemical workstation consists of a working electrode, counter electrode Pt plate, and standard calomel electrode (SCE) as a reference electrode (Ag/AgCl)), which were dipped in a 0.1 mol/L tetra butyl ammonium hexafluorophosphate (Bu4NPF6) in acetonitrile solution [17, 18]. The J-V characteristics of the fabricated OPV devices were measured using an AM1.5 simulator system manufactured by SCIENCE TECH, Canada.

3. RESULTS AND DISCUSSION

3.1. UV–Vis Absorption Spectroscopy

Figure 2 displays the typical UV–Vis absorption spectra of P3HT: ICxA dilute solutions and thin films at different weight ratios. The spectra of the dilute solutions showed the strongest absorption in the visible region at 454 nm, which attribute to the π–π* transitions of the polymer in the blends, with a small peak at 310 nm, as shown in Figure 2a. The spectra of the annealed thin films at 140°C for 5 min were much broader compared to those of solutions, as shown in Figure 2b. Strong peaks were observed at 511 nm with two pronounced shoulders at 529 and 604 nm, as well as, two peaks at 325 and 253 nm, which are attributed to the contribution of the polymer and fullerene in the blend. In addition, the absorption edges were significantly red-shifted in the thin films, which can be ascribed to the more ordered aggregates, more ordered inter-chain stacking, and enhanced crystallinity in the solid film [19]. As the fullerene ratio increased, the thin films exhibited a blue shift in the absorption spectra, and the energy gap increased as well. This shift is attributed to reduced inter-chain interactions due to the presence of fullerene, where fullerene molecules isolate chains of P3HT from their neighbors [20] [21]. Therefore, the donor-to-acceptor composition ratio influences the electronic properties of the blends [20, 21].

By using Tauc's formula [22], the optical energy gap (Eg) was estimated by extrapolating the linear fitted line in the $(\alpha h\nu)^2$ vs. hν plots near the fundamental absorption edge region, as shown in Figure 3a for solutions and Figure 3b for thin films. The Tauc method is based on the assumption that the absorption coefficient (α) can

[Downloaded from nezarat.iust.ac.ir on 2025-07-18]

[DOI: 10.22068/ijmse.3147]

be expressed by the following Equation [23, 24]:

$$\alpha h\nu = K((h\nu - E_g))^m \quad (1)$$

Where K is an energy-independent constant, hν is the energy of the incident photons, and Eg is the optical energy gap. The m factor depends on the nature of the electron transition and is equal to 1/2 for the direct and 2 for the indirect transition band gap. According to the Beer-Lambert law, the absorption coefficient is given by the following Equation [25]:

$$\alpha = 2.303A/t \quad (2)$$

Where A absorbance of the samples, t is the thickness of the samples estimated for thin films (125 nm), and for solution samples (1 cm). The optical energy gap results obtained using Tauc's equation and the absorption edge onset are summarized in Table 1. These results indicate that the energy gap of the polymer increases with increasing fullerene content in the blend. The energy gap values of the materials in both techniques were similar. Pure P3HT has a direct transition band gap, which agrees with previous results [26, 27].

3.2. Photoluminescence (PL) Spectroscopy

To study the internal domain structure of P3HT, using a 500 nm excitation wavelength the emission and absorption spectra of the pure P3HT solution and the thin film were shown in Figure 4a and 3b, respectively.

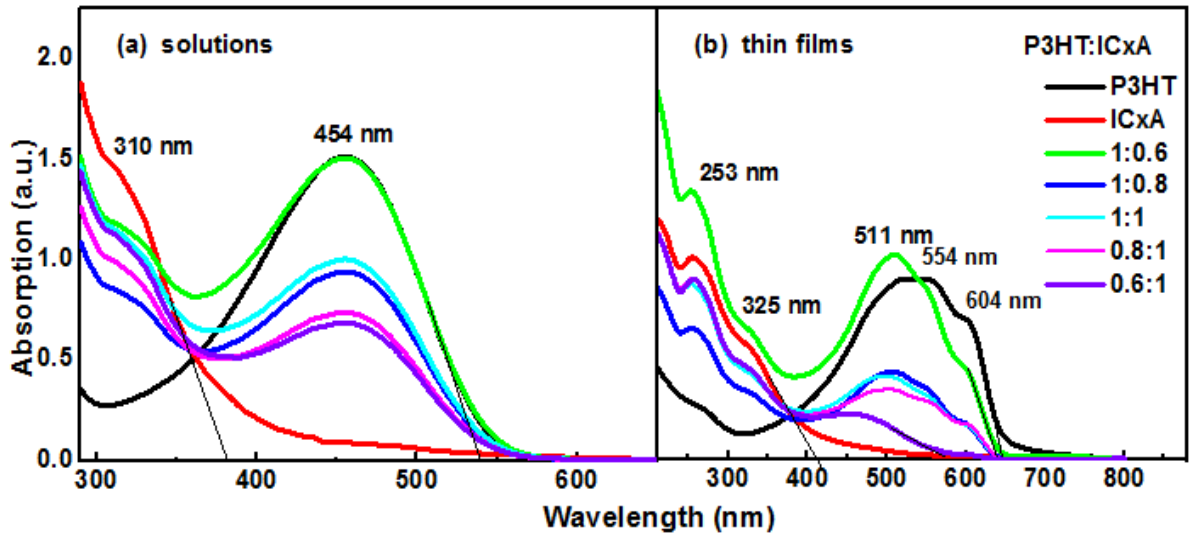

Fig. 2. Absorption spectra of P3HT, ICxA, and P3HT:ICxA blends, (a) as solutions, and (b) as a thin films. The linear part of the plot is extrapolated to the x-axis.

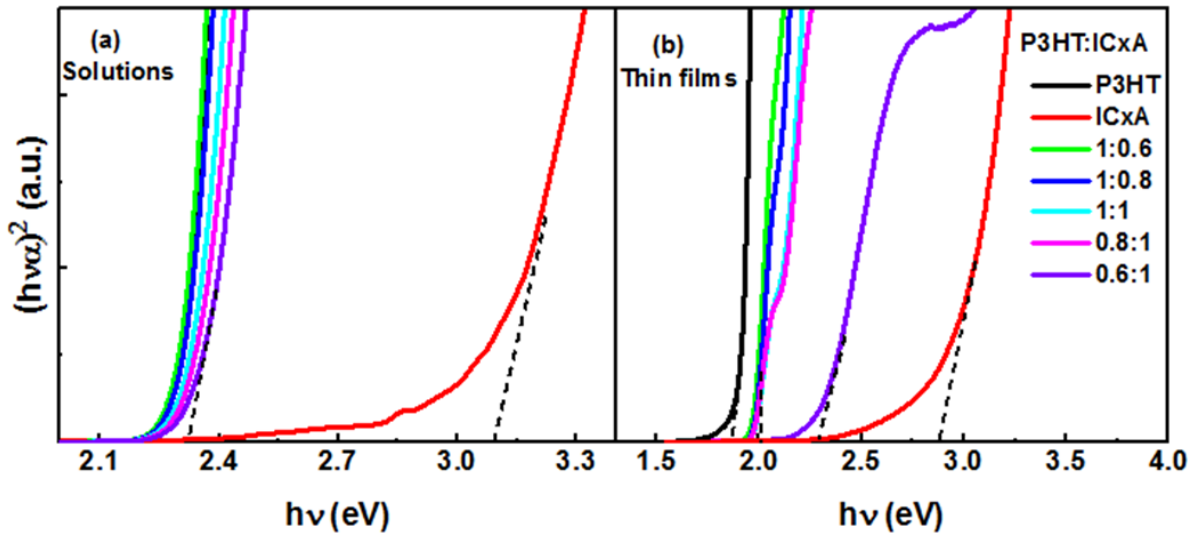

Fig. 3. The estimated Eg using Tauc's equation for samples, (a) in case solution and (b) in case thin film. The linear part of the plot is extrapolated to the x-axis.

[Downloaded from nezarat.iust.ac.ir on 2025-07-18]

[DOI: 10.22068/ijmse.3147]

Table 1. The E_g values for P3HT:ICxA blends using Tauc's equation and absorption edge onset.

P3HT:ICxA	E_g (onset) (eV) Thin film	E_g (Tauc) (eV) Thin film	E_g (onset) (eV) Solution	E_g (Tauc) (eV) Solution
P3HT	1.93	1.87	2.3	2.28
1:0.6	1.93	1.95	2.3	2.24
1:0.8	1.95	1.96	2.3	2.26
1:1	1.95	1.97	2.3	2.27
0.8:1	1.95	1.98	2.31	2.29
0.6:1	2.1	2.3	2.32	2.23
ICxA	3.08	2.88	3.1	3.1

In Figure 4a, the normalized absorption spectrum (black line) of the P3HT solution is a broad band with a peak at 454 nm, mainly related to the intra-chain states of the individual P3HT chains, aggregation between chains is considered negligible, which leads to a structure-free absorption spectrum. The emission spectrum (red line) is narrower and displays a vibrational progression, with a peak at 582 nm (2.13 eV), indicating a Stokes shift, i.e., the energy difference between the emission maximum and the absorption edge at 544 nm (2.28 eV) is 0.15 eV [28]. On the other hand, the absorption and emission spectra of the P3HT thin film are considerably different from those of P3HT in solution, as shown in Figure 4b, which displays the characteristic transitions associated with interchain exciton delocalization and significant coupling to vibrations. Generally, spin-coated films show more pronounced 0-0, 0-1, and 0-2 vibronic features, suggesting a higher ordering in the polymer phase [29]. The 0-0 transition represents the intra-chain interactions of P3HT, whereas the 0-1 and 0-2 bands refer to the inter-chain interactions [30]. The absorption spectrum of the P3HT thin film (black line) was strongly red-shifted in the peak positions compared to that in solution, with a maximum at 554 nm corresponding to the 0-1 transition. In addition, displays two pronounced shoulders at 529 and 604 nm, corresponding to 0-2 and 0-0 vibronics, respectively. In contrast, the emission spectrum (red line) of the P3HT thin film displayed two pronounced peaks at 672 nm (1.84 eV) and 698 nm (1.77 eV). The appearance of the peaks is an indication of the ordered structure after the self-assembly of the P3HT polymer. The ordered aggregation of P3HT chains in the thin film is associated with interchain delocalized excitons resulting from the π–π stacking of the P3HT chains [19]. Photoluminescence (PL) measurements of the blends were recorded in solution and thin films, as shown in Figures 5a and 4b, respectively. The blend solution spectra gradually decrease as the ICxA ratio increases, with a maximum peak at 582 nm. In the case of the thin films, the emission spectra were red-shifted compared to the spectra of the solutions, with two maximum peaks at 670 and 698 nm. The emission spectra demonstrated a Stokes shift of 0.15 eV. As the ratio of ICxA in the blend increased, the spectra are blue-shifted compared with the emission spectrum of the P3HT film. In contrast to that of the pure P3HT spectrum, the intensity of the 0-0 vibronic peak corresponds to the maximum emission peak. It has been observed that the I0–0/I0–1 value of blend films is less than 1, indicating that H-aggregation dominates [19, 31].

3.3. Raman Spectroscopy

We now turn to Raman spectroscopy to obtain a deeper understanding of the crystallinity of conjugated polymers. Raman spectra of thin films are shown in Figure 6. The samples were excited with a laser operating at a wavelength of 532 nm. The Stokes-Raman shift is a symmetric stretching mode containing several peaks. The peaks in the Raman spectra of the P3HT and P3HT: ICxA blend films, at 1465 cm^{-1} and 1401 cm^{-1} are attributed to the C=C symmetric stretching and C–C skeletal stretching of the thiophene ring, respectively. Other peaks at 1208 cm^{-1} and 1100 cm^{-1} correspond to the inter-ring C–C stretch mode and C–C inter-ring stretching with the C–H bending mode, respectively [32, 33]. It was found that an increase in the ICxA content leads to an increase in the peak intensity of the C=C and C–C modes, and the peak of the C–C mode shifts towards a lower wavenumber and a decrease in its FWHM. The crystallization of the P3HT: ICxA films was inferred from the fact that the Raman intensity in the main mode (C=C) is higher,

[Downloaded from nezarat.iust.ac.ir on 2025-07-18]

[DOI: 10.22068/ijmse.3147]

sharper, and has symmetrical broadening, in addition to a smaller FWHM compared to those of the P3HT spectrum. To determine the heights of the intensities and FWHM parameters, the symmetric stretching peak was fitted with a Gaussian function. The results related to Raman spectra are listed in Table 2. The positions of the C=C and C–C stretch modes as well as the relative intensity ($I_{C=C}/I_{C-C}$) indicate the backbone conformation and molecular order of P3HT in the films [33]. By taking the ratio of intensities ($I_{C=C}/I_{C-C}$), we found that the P3HT film showed a value of 7.6, whereas the blend films had a smaller average value of 7.46, with the smallest value being 6 for a 1:0.6 ratio.

The small values of ($I_{C=C}/I_{C-C}$) indicate more conformation; hence, high aggregation, while the large values of the relative intensity suggest a more twisted conformation of P3HT chains [34, 35].

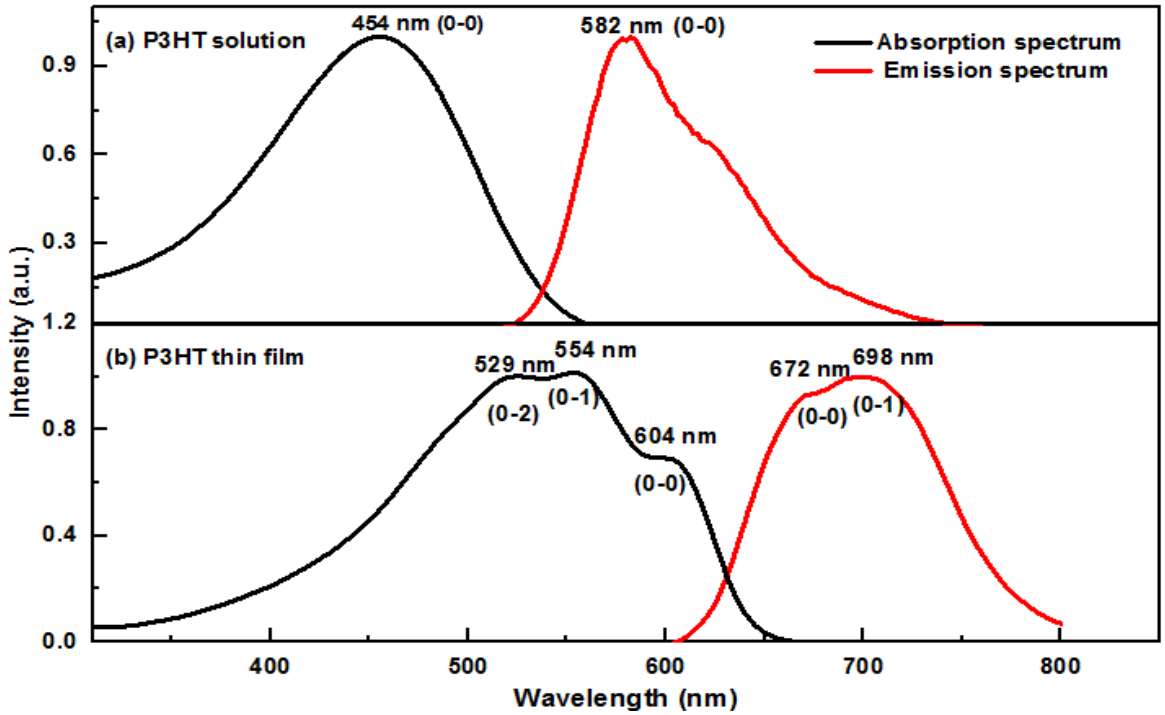

Fig. 4. Normalized emission (red lines) and absorption (black lines) spectra of P3HT excited at wavelengths of 500 nm, (a) solutions, and (b) thin films.

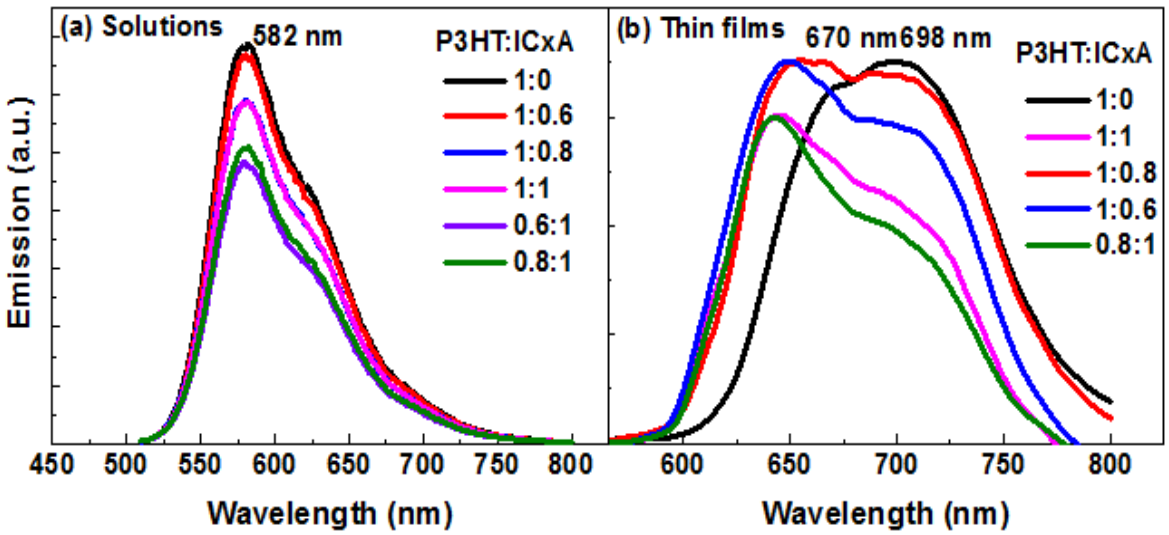

Fig. 5. Photoluminescence spectra of P3HT:ICxA blends excited at wavelengths of 500 nm, (a) as solutions, (b) as a thin films.

[Downloaded from nezarat.iust.ac.ir on 2025-07-18]

[DOI: 10.22068/ijmse.3147]

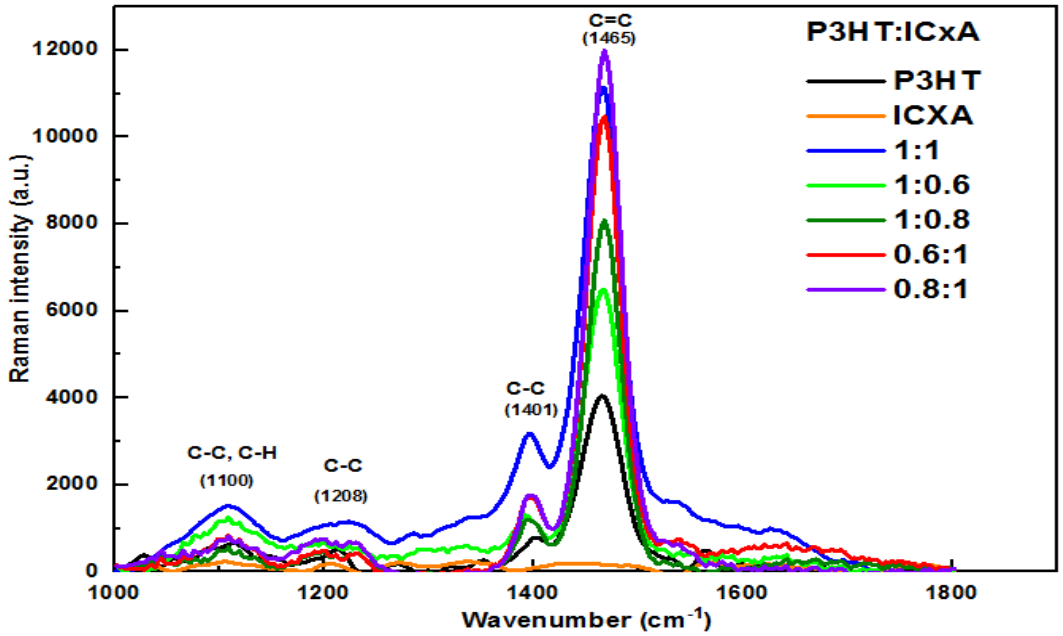

Fig. 6. Raman spectra of P3HT, ICxA, and P3HT: ICxA films, which obtained laser excitation at 532 nm.

Table 2. The Raman parameters, and positions of symmetric stretch (C=C) and inter-ring (C-C), ($I_{C=C}/I_{C-C}$), and FWHM of P3HT: ICxA thin films.

P3HT:ICxA	Pos. C=C (cm^{-1})	Pos. C–C (cm^{-1})	$I_{C=C}/I_{C-C}$	FWHM C=C (cm^{-1})
P3HT	1465	1401	7.6	48.5
1:0.6	1465	1395	6	51
1:0.8	1468	1395	7.8	44.6
1:1	1465	1395	6.8	46.6
0.8:1	1468	1395	9.8	42.7
0.6:1	1468	1395	6.9	45.1
ICxA	-	-	-	-

Upon blending the polymer (P3HT) with the fullerene acceptor (ICxA), no apparent shift in the peak position was observed. This indicates that the acceptor material is loaded onto the polymer backbone without much alteration in the conjugation length of the polymer [32].

3.4. X-Ray Diffraction (XRD)

Figure 7a displays the X-ray diffraction (XRD) patterns of the P3HT, ICxA, and P3HT: ICxA films, whereas Figure 7b shows the effect of fullerene on thin film crystallization through line broadening and FWHM. The peak position, intensity, FWHM of the peak, and d-spacing are considered significant parameters in the XRD spectra, which are summarized in Table 3. From the X-ray diffraction pattern, the detected peak corresponded to the (100) reflection [33]. The crystallite size (D) was calculated from the diffraction pattern using the Scherrer equation [36, 37]:

$$D = \frac{0.9\,\lambda}{\beta\,\cos\theta} \quad (3)$$

Where λ is the X-ray wavelength, β is the FWHM of the peaks, and θ is the Bragg angle. According to Winokur's proposition for the unit cell, lattice constant (a) is equivalent to the chain-chain interlayer distance at (100) [38, 39].

The results indicate that the crystallite sizes of P3HT: ICxA with 1:0.8 and 1:0.6 ratios were significantly larger than those of the other samples. As depicted in the results, the blend films exhibited a significant decrease in the FWHM and d-spacing, and an increase in the crystallite size, indicating an increase in the ordering of the alkyl chains within the main thiophene chains [40]. We note that the ICxA is an amorphous substance. As shown in Figure 7b, the diffraction peaks became more regular, sharp, and symmetrical broadening when ICxA was added to P3HT.

[Downloaded from nezarat.iust.ac.ir on 2025-07-18]

[DOI: 10.22068/ijmse.3147]

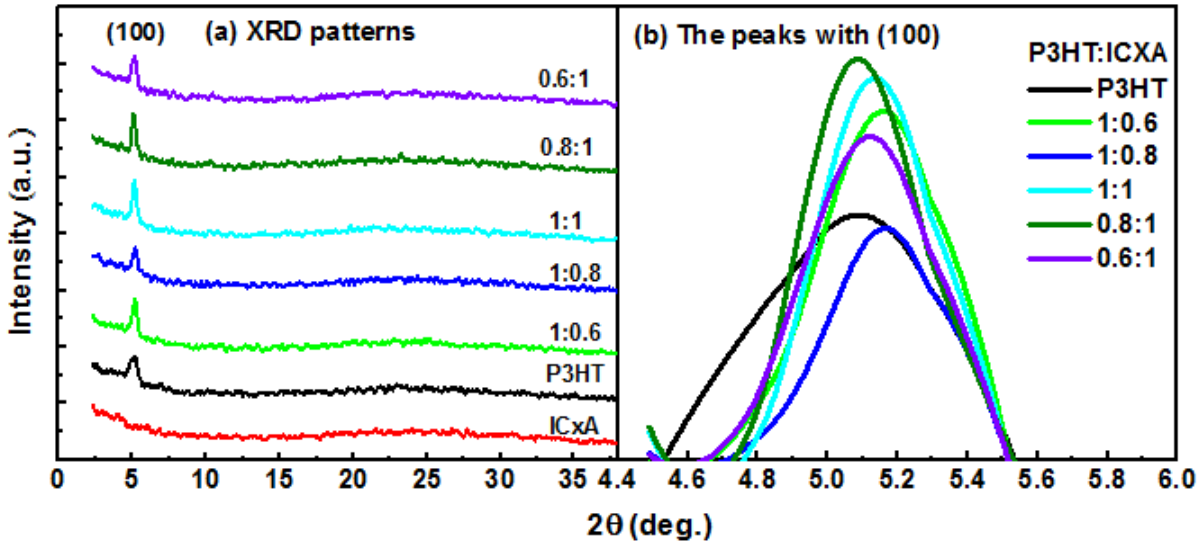

Fig. 7. (a) XRD patterns of the P3HT, ICxA and various composite ratios of P3HT:ICxA films. (b) The peaks of XRD patterns with (100) reflection.

Table 3. The basic parameters of X-ray diffraction patterns, in addition the crystallite size (D).

P3HT:ICxA	2θ (deg.)	FWHM (Rad.)	d-spacing (Å)	D (Å)
P3HT	5.09	0.7680	17.33967	108.1
1:0.6	5.15	0.2362	17.14660	351.5
1:0.8	5.22	0.2160	16.90558	384.4
1:1	5.11	0.2640	17.27473	314.5
0.8:1	5.09	0.2880	17.34691	288.3
0.6:1	5.11	0.3840	17.26786	216.2
ICxA	amorphous	-	-	-

3.5. Electrochemical Characterization

Cyclic voltammetry (CV) measurements were performed on an electrochemical workstation. Figure 8 shows the CV curves of pure and blended thin films with varying blending ratios. The potential was scanned from -3 to +3 V at a scan rate of 20 mV s^{-1}. The onset of oxidation (E_{ox}) potential represents the first observed anodic signal, whereas the reduction (E_{red}) potential represents the first observed cathodic signal, which was used to calculate the HOMO and LUMO energy levels. The E_g of the materials was calculated according to the following equations [41, 42]:

$$E_{HOMO} = -e(E_{ox} + 4.8)(eV) \quad (4)$$

$$E_{LUMO} = -e(E_{red} + 4.8)(eV) \quad (5)$$

$$E_g = (E_{LUMO} - E_{HOMO})(eV) \quad (6)$$

Where 4.8 is the ferrocene energy level relative to the vacuum level when the ferrocenium/ferrocene (Fc/Fc^+) redox couple is used as an internal standard [41]. The (HOMO)/(LUMO) energy levels of P3HT and ICxA were calculated to be -5.5/-3.3 and -6.8/-3.87 eV, respectively. On the other hand, the HOMO and LUMO levels of blends are sandwiched between those of the pure materials. Notably, the HOMO levels of all blends vary from -5.8 to -6.08 eV, which is closer to P3HT, while their LUMO levels range from -3.78 to -3.84 eV, which is closer to ICxA as summarized in Table 4.

Table 4. Cyclic voltammetry results, E_g, E_{ox}, E_{red}, and E_{HOMO}/E_{LUMO} levels of P3HT: ICxA blend thin films.

P3HT:ICxA	E_{ox} (eV)	E_{red} (eV)	E_{HOMO}/ E_{LUMO} (eV)	E_g (eV)
P3HT	0.70	-1.50	-5.50/-3.30	2.20
1:0.6	1	-1.01	-5.80/-3.78	2.02
1:0.8	1.02	-1.04	-5.82/-3.76	2.06
1:1	1.07	-0.99	-5.87/-3.81	2.02
0.8:1	1.08	-0.97	-5.88/-3.83	2.05
0.6:1	1.10	-0.96	-5.90/-3.84	2.06
ICxA	2	-0.93	-6.80/-3.87	2.93

[Downloaded from nezarat.iust.ac.ir on 2025-07-18]

[DOI: 10.22068/ijmse.3147]

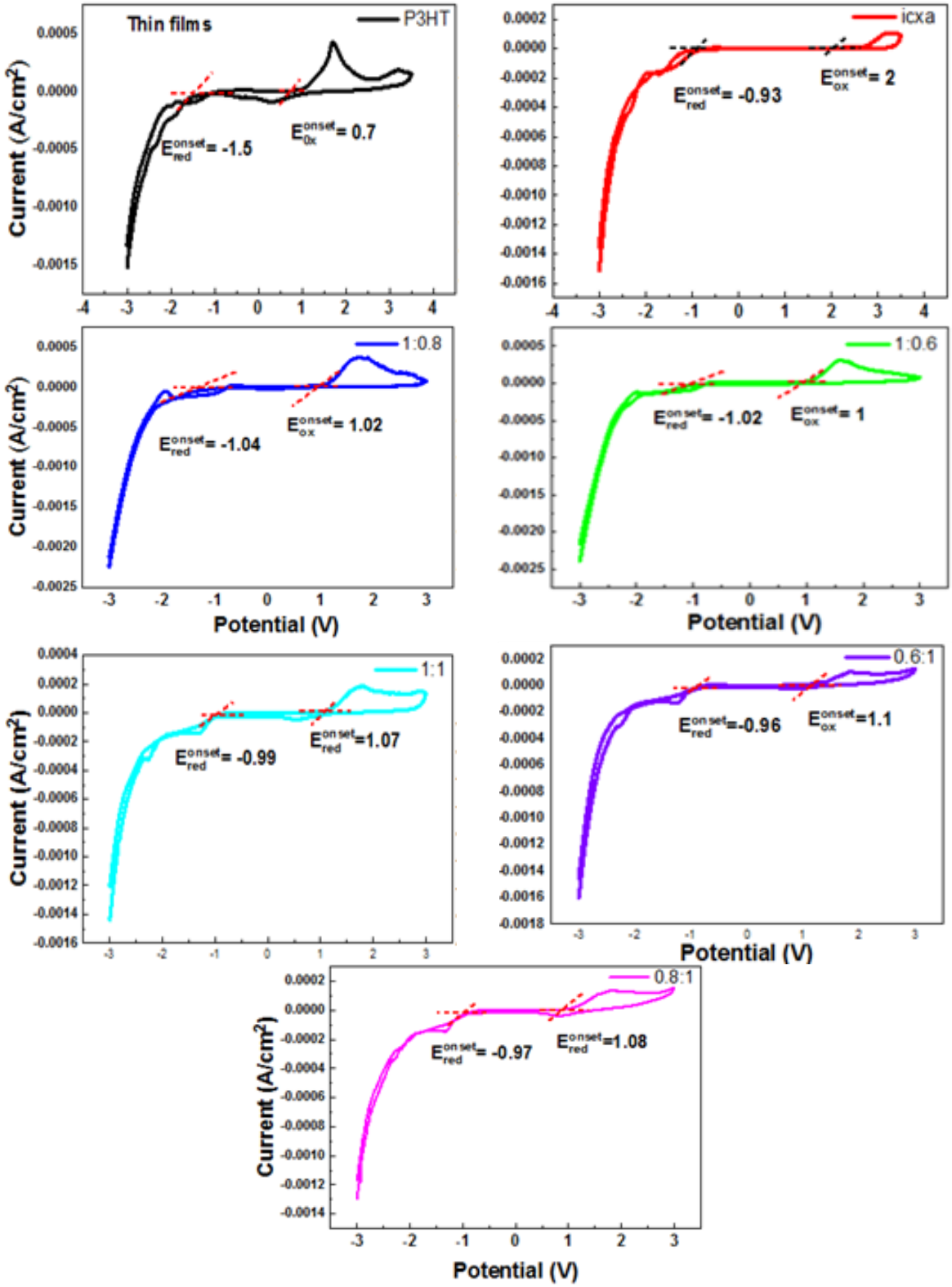

Fig. 8. Cyclic voltammetry curves for P3HT:ICxA blends. Cross-dashed lines were used to estimate position of Ered and Eox.

The LUMO position of pristine P3HT has been reported in a broad range of -3.53 to -2.70 eV, while its HOMO position lies within a narrow range of -4.92 to -5.20 eV [18]. The E_g values

[Downloaded from nezarat.iust.ac.ir on 2025-07-18]

[DOI: 10.22068/ijmse.3147]

measured using the CV technique were close to the optical gaps derived from the UV-Vis absorption spectra. The results indicate that the difference (E_{LUMO} (P3HT)-E_{LUMO} (ICxA)) decreased after blending, leading to create a driving force at the interface between the two materials, which is strong enough to separate the charge carriers of photo-generated excitons [43].

Figure 9 shows the energy band diagrams of materials used in fabricating the devices. The difference between the work function of Al ($\phi_{(Al)}$= 4.2 eV) and the electron affinity (Ea) of ZnO (Ea (ZnO)= 4.5 eV), as well as, the difference between the work functions of ITO ($\phi_{(ITO)}$= 4.8 eV) and ionization potential (Ip) of PEDOT: PSS (Ip (PEDOT:PSS)= 5.2 eV). Both of ZnO and PEDOT: PSS layers lead to form ohmic contact between electrodes to avoid the opposite collection of charge carriers [44, 45].

In our devices, holes were injected into the HOMO of PEDOT: PSS, and electrons were injected into the energy bands of ZnO. Due to the formed barriers (E_{LUMO} (ICxA)–Ea (ZnO)) prevents the transfer of electrons to the anode electrode and barrier (E_{HOMO} (P3HT)-E_{HOMO} (PEDOT: PSS)) prevents the transfer of holes to the cathode electrode. The holes injected into the ITO can be blocked by ZnO because of the higher ionization potential Ip (ZnO) compared to Ip (PEDOT: PSS), leading to the transfer of holes to P3HT when Ip (PEDOT: PSS) and Ip (P3HT) are equivalents. The electrons injected into an aluminum cannot be transferred to PEDOT: PSS because Ea (PEDOT: PSS) is less than Ea (ZnO), but they can be trapped on ICxA owing to the lower Ea (ICxA) than that of Ea (ZnO) [46, 47]. The difference between the E_{HOMO} (D) of the electron donor material and E_{LUMO} (A) of the electron acceptor material is related to the open-circuit voltage (V_{OC}) of the organic solar cells. Therefore, an increase in E_{HOMO} (P3HT)-E_{LUMO} (ICxA) leads to an increase in V_{OC}, thereby enhancing the efficiency of photovoltaic devices despite the reduced absorption of photons because of an increase in the bandgap [48, 49].

3.6. J–V Characteristics

Under different blending ratios of the active layer, the solar cell's performance with 0.06 cm^2 was investigated using the AM1.5 Solar Simulator. The measurements were conducted immediately after the device was manufactured to avoid the oxidation problem.

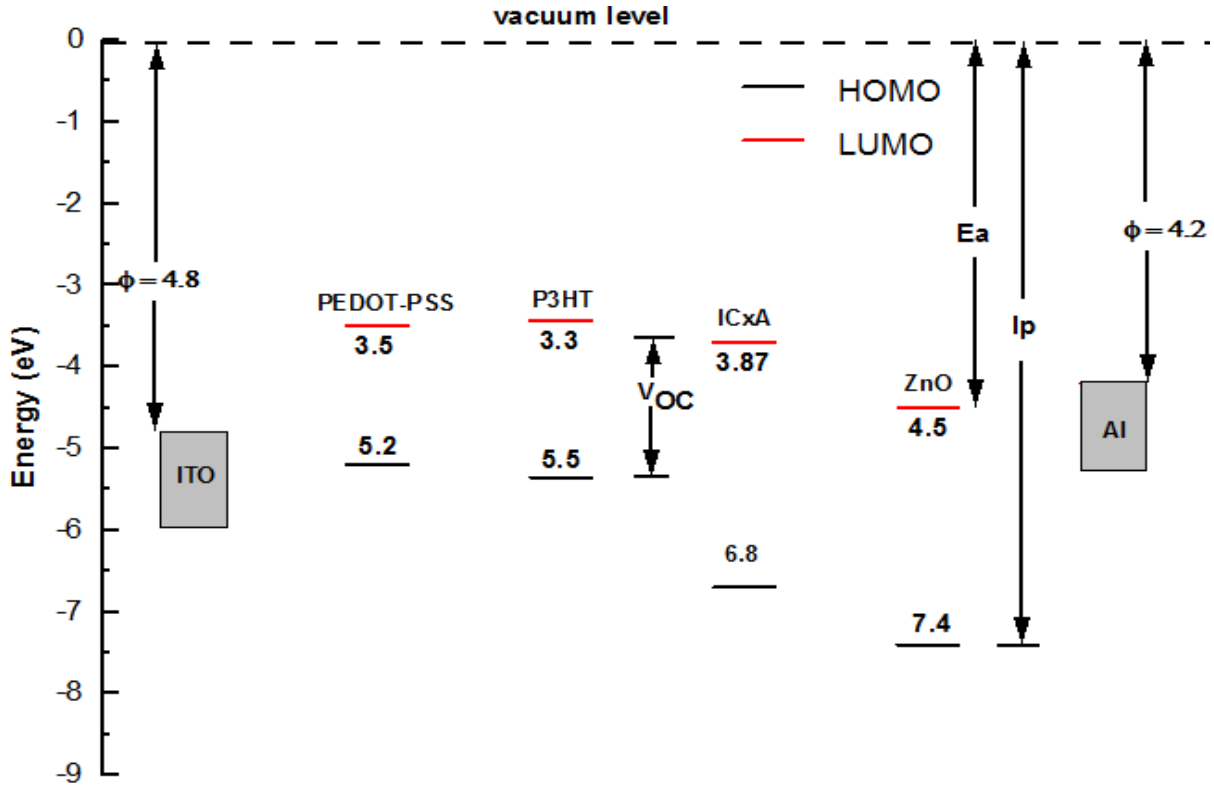

Fig. 9. Schematic of energy band diagram of organic solar cell.

[Downloaded from nezarat.iust.ac.ir on 2025-07-18]

[DOI: 10.22068/ijmse.3147]

The J–V characteristics of the ITO/ PEDOT: PSS/ P3HT: ICxA/ZnO/Al device were tested, as shown in Figure 10. The photovoltaic performance parameters such as the open-circuit voltage (V_{OC}), the short-circuit current density (J_{SC}), the fill factor (FF), the series resistance (R_s), and the shunt resistance (R_{sh}) were determined, as summarized in Table 5. The best device performance was recorded for the P3HT: ICxA (1:0.6) with PCE= 1.21%, FF= 39.51, J_{SC}= 5.71 mA.cm^{-2} and V_{OC}= 0.534V. We also calculated the voltage loss, which is given by $V_{loss}= E_g/q-V_{OC}$, where q is the elementary charge [50]. P3HT: ICxA devices display a reduction in PCE with increasing ICxA content, owing to their low J_{SC} and FF values, despite their higher open-circuit voltage values, which are attributed to limited photon harvesting by the active layer and high voltage loss due to carrier recombination. The low values of R_s and large values of R_{sh} lead to improved FF, which is attributed to the strong molecular stacking during active layer formation, leading to reduced interfacial resistance between layer structures and reduced leakage current owing to defects [51].

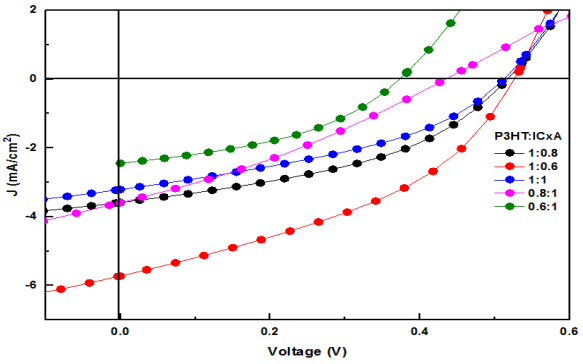

Fig. 10. Current density–voltage (J–V) curves for a spin-coated binary active layers (P3HT: ICxA) based organic solar cells under illumination.

4. CONCLUSIONS

This study provides valuable information on the effect of the ICxA ratio in the P3HT: ICxA system, which may be useful in photovoltaic (PV) systems. Solutions, thin films, and OSCs based on P3HT were studied by adding ICxA at different blending ratios. Optical absorption spectra displayed a reduction in their intensities upon increasing the fullerene ratio, with a blue shift in the main peak. However, the 1:0.6 ratio showed an increase in the intensity of the absorption spectrum compared to the P3HT intensity for both the solution and thin film samples. In addition, the 1:0.6 ratio exhibited higher efficiency and lower voltage losses. On the other hand, the emission spectra demonstrate a reduction by increasing the fullerene ratio; this allows the excitons to reach the interface between the polymer and fullerene to be separated into free charges before the processes of capture or recombination. A small intensity ratio ($I_{C=C}/I_{C-C}$) along with a low value of full width high maximum (FWHM) of Raman spectra are associated with increased composition aggregation and conformation. The results were further confirmed by Raman spectroscopy, XRD, and power conversion efficiency measurements. The reduction in the band offset between the LUMO energy level of the acceptor and the LUMO energy level of the donor increases the open-circuit voltage of the OPV device and improves the charge separation processes in the devices. The solar cell performance demonstrated a decrease in PCE with a further increase in the fullerene ratio in the blend.

ACKNOWLEDGMENTS

The authors thank Basra University for its financial support. The authors would like to offer their thanks to the University of Basrah Nanotechnology Lab for the technical support of the XRD, Raman, and solar cells measurements.

FUNDING

This research was supported by the Basra University Research Science College's Discovery Projects funding scheme.

Table 5. The electrical parameters for the organic solar cells with different weight ratios.

P3HT:ICxA	V_{OC} V	Jsc mA/cm^2	FF %	Rs Ω	Rsh Ω	PCE %	V_{loss} V
1:0.6	0.53	5.7	39	171	5089	1.21	1.39
1:0.8	0.54	3.5	40	311	8245	0.78	1.40
1:1	0.53	3.2	37	337	7136	0.65	1.41
0.8:1	0.45	3.5	29	1125	4558	0.48	1.49
0.6:1	0.38	2.2	33	407	1558	0.38	1.72

[Downloaded from nezarat.iust.ac.ir on 2025-07-18]

[DOI: 10.22068/ijmse.3147]

CONFLICT OF INTEREST

The authors have declared that this research was conducted without any commercial or financial relationships that might be construed as conflicts of interest.

REFERENCES

[1]. Heeger, A.J., "Semiconducting and metallic polymers: the fourth generation of polymeric materials." J. phys. Chem. B., 2001, 105, 8475-8491.

[2]. Shirakawa, H., Louis, E.J., MacDiarmid, A.G., Chiang, C.K. and Heeger, A.J., "Synthesis of electrically conducting organic polymers: halogen derivatives of polyacetylene, (CH) x." J. Chem. Soc., Chem. Commun., 1977, 16, 578-580.

[3]. Kearns, D. and Calvin, M., "Photovoltaic effect and photoconductivity in laminated organic systems." J. chem. phys., 1958, 29, 950-951.

[4]. Tang, C.W., "Two-layer organic photovoltaic cell." Appl. Phys. Lett., 1986, 48, 183-185.

[5]. Yu, G., Gao, J., Hummelen, J.C., Wudl, F. and Heeger, A.J., "Polymer photovoltaic cells: enhanced efficiencies via a network of internal donor-acceptor heterojunctions." Sci., 1995, 270, 1789-1791.

[6]. Kim, J.Y., Lee, K., Coates, N.E., Moses, D., Nguyen, T.Q., Dante, M. and Heeger, A.J., "Efficient tandem polymer solar cells fabricated by all-solution processing." Sci., 2007, 317, 222-225.

[7]. Brabec, C.J. and Durrant, J.R., "Solution-processed organic solar cells." MRS bulletin, 2008, 33, 670-675.

[8]. Hart, A.S., Andersen, T.R., Griffith, M.J., Fahy, A., Vaughan, B., Belcher, W.J. and Dastoor, P.C., "Roll-to-roll solvent annealing of printed P3HT: IC XA devices." RSC adv., 2019, 9, 42294-42305.

[9]. He, Y., Chen, H.Y., Hou, J. and Li, Y., "Indene− C_{60} bisadduct: a new acceptor for high-performance polymer solar cells." J. Ameri. Chem. Soc., 2010, 132, 1377-1382.

[10]. Zhao, G., He, Y. and Li, Y., "6.5% efficiency of polymer solar cells based on poly (3-hexylthiophene) and indene-C_{60} bisadduct by device optimization." Adv. Mater., 2010, 22, 4355-4358.

[11]. Cooling, N.A., Barnes, E.F., Almyahi, F., Feron, K., Al-Mudhaffer, M.F., Al-Ahmad, A., Vaughan, B., Andersen, T.R., Griffith, M.J., Hart, A.S. and Lyons, A.G., "A low-cost mixed fullerene acceptor blend for printed electronics." J. Mater. Chem. A., 2016, 4, 10274-10281.

[12]. Almyahi, F., Andersen, T.R., Fahy, A., Dickinson, M., Feron, K., Belcher, W.J. and Dastoor, P.C., "The role of surface energy control in organic photovoltaics based on solar paints." J. Mater. Chem. A., 2019, 7, 9202-9214.

[13]. Reichenberger, M., Kroh, D., Matrone, G.M., Schötz, K., Pröller, S., Filonik, O., Thordardottir, M.E., Herzig, E.M., Bässler, H., Stingelin, N. and Köhler, A., "Controlling aggregate formation in conjugated polymers by spin-coating below the critical temperature of the disorder–order transition." J. Polym. Sci. Part B: Polym. Phys., 2018, 56, 532-542.

[14]. Xiao, T., Cui, W., Anderegg, J., Shinar, J. and Shinar, R., "Simple routes for improving polythiophene: fullerene-based organic solar cells." Org. Electron., 2011, 12, 257-262.

[15]. Almyahi, F., Andersen, T.R., Cooling, N., Holmes, N.P., Fahy, A., Barr, M.G., Kilcoyne, D., Belcher, W. and Dastoor, P.C., "Optimization, characterization and upscaling of aqueous solar nanoparticle inks for organic photovoltaics using low-cost donor: acceptor blend." Org. Electron., 2018, 52, 71-78.

[16]. Motaung, D.E., Malgas, G.F., Nkosi, S.S., Mhlongo, G.H., Mwakikunga, B.W., Malwela, T., Arendse, C.J., Muller, T.F. and Cummings, F.R., "Comparative study: the effect of annealing conditions on the properties of P3HT: PCBM blends." J. Mater. Sci., 2013, 48, 1763-1778.

[17]. Kuila, B.K., Park, K. and Dai, L., "Soluble P3HT-grafted carbon nanotubes: synthesis and photovoltaic application." Macromolecules, 2010, 43, 6699-6705.

[18]. Acevedo-Peña, P., Baray-Calderón, A., Hu, H., González, I. and Ugalde-Saldivar, V.M., "Measurements of HOMO-LUMO levels of poly (3-hexylthiophene) thin films

[Downloaded from nezarat.iust.ac.ir on 2025-07-18]

[DOI: 10.22068/ijmse.3147]

by a simple electrochemical method." J. Solid State. Ele. chem., 2017, 21, 2407-2414.

[19]. Chaudhary, V., Pandey, R.K., Prakash, R. and Singh, A.K., "Self-assembled H-aggregation induced high performance poly (3-hexylthiophene) Schottky diode." J. Appl. Phys., 2017, 122, 225501.

[20]. Dang, M.T., Hirsch, L., Wantz, G. and Wuest, J.D., "Controlling the morphology and performance of bulk heterojunctions in solar cells. Lessons learned from the benchmark poly (3-hexylthiophene): [6, 6]-phenyl-C61-butyric acid methyl ester system." Chem. Rev., 2013, 113, 3734-3765.

[21]. Yamagata, H. and Spano, F.C., "Interplay between intrachain and interchain interactions in semiconducting polymer assemblies: The HJ-aggregate model." J. chem. Phys., 2012, 136, 184901.

[22]. Tauc, J. and Menth, A., "States in the gap." J. non-cry. sol., 1972, 8, 569-585.

[23]. Makuła, P., Pacia, M. and Macyk, W., "How to correctly determine the band gap energy of modified semiconductor photocatalysts based on UV–Vis spectra." J. Phys. Chem. Lett, 2018, 9, 6814-6817.

[24]. Saeidi, M., Abrari, M. and Ahmadi, M., "Fabrication of dye-sensitized solar cell based on mixed tin and zinc oxide nanoparticles." Appl. Phys. A, 2019, 125, 1-9.

[25]. Bahadur, J. and Pal, K., "Efficient photodegradation of organic dye using anatase TiO_2 plants as catalyst." Electron. Mater. Lett., 2017,13, 463-470.

[26]. Mousavi, S.L., Jamali-Sheini, F., Sabaeian, M. and Yousefi, R., et al. "Enhanced solar cell performance of P3HT: PCBM by SnS nanoparticles." Sol. Energy, 2020, 199, 872-884.

[27]. Çaldıran, Z., Erkem, Ü., Baltakesmez, A. and Biber, M., "Effects of the PENTACENE as doping material on the power conversion efficiency of P3HT: PCBM based ternary organic solar cells." Phys. B Condens. Matter, 2021, 607, 412859.

[28]. Banerji, N., Cowan, S., Vauthey, E. and Heeger, A.J., "Ultrafast relaxation of the poly (3-hexylthiophene) emission spectrum." J. Phys. Chem. C, 2011, 115, 9726-9739.

[29]. Wilken, S., Scheunemann, D., Dahlström, S., Nyman, M., Parisi, J. and Österbacka, R., "How to reduce charge recombination in organic solar cells: There are still lessons to learn from P3HT: PCBM." Adv. Electron. Mater., 2021, 7, 2001056.

[30]. Mahakul, P.C. and Mahanandia, P., "RGO induced structural and microstructural properties of P3HT in the performance and stability of polymer solar cells." Mat. Res. Exp., 2019, 6, 125338.

[31]. Spano, F.C., "The spectral signatures of Frenkel polarons in H-and J-aggregates." Acc. Chem. Res., 2010, 43, 429-439.

[32]. Falke, S., Eravuchira, P., Materny, A. and Lienau, C., "Raman spectroscopic identification of fullerene inclusions in polymer/fullerene blends." J. Raman Spectrosc., 2011, 42, 1897-1900.

[33]. Kim, Y.S., Lee, Y., Kim, J.K., Seo, E.O., Lee, E.W., Lee, W., Han, S.H. and Lee, S.H., "Effect of solvents on the performance and morphology of polymer photovoltaic devices." Curr. Appl. Phys., 2010, 10, 985-989.

[34]. Wu, L., Casado, S., Romero, B., Otón, J.M., Morgado, J., Müller, C., Xia, R. and Cabanillas-Gonzalez, J., "Ground state host–guest interactions upon effective dispersion of regioregular poly (3-hexylthiophene) in poly (9, 9-dioctylfluorene-alt-benzothiadiazole)." Macromolecules, 2015, 48, 8765-8772.

[35]. Gao, Y. and Grey, J.K., "Resonance chemical imaging of polythiophene/fullerene photovoltaic thin films: mapping morphology-dependent aggregated and unaggregated C=C species." J. Ameri. Chem. Soc., 2009, 131, 9654-9662.

[36]. Monshi, A., Foroughi, M.R. and Monshi, M.R., "Modified Scherrer equation to estimate more accurately nano-crystallite size using XRD." World J. Nano Sci. Eng., 2012, 2, 154-160.

[37]. Abrari, M., Ghanaatshoar, M., Hosseiny Davarani, S.S., Moazami, H.R. and Kazeminezhad, I., "Synthesis of SnO_2 2 nanoparticles by electrooxidation of tin in quaternary ammonium salt for application

[Downloaded from nezarat.iust.ac.ir on 2025-07-18]

[DOI: 10.22068/ijmse.3147]

in dye-sensitized solar cells." Appl. Phys. A, 2017, 123, 1-9.
[38]. Prosa, T.J., Winokur, M.J., Moulton, J., Smith, P. and Heeger, A.J., "X-ray structural studies of poly (3-alkylthiophenes): an example of an inverse comb." Macromolecules, 1992, 25, 4364-4372.
[39]. Zen, A., Saphiannikova, M., Neher, D., Grenzer, J., Grigorian, S., Pietsch, U., Asawapirom, U., Janietz, S., Scherf, U., Lieberwirth, I. and Wegner, G., "Effect of molecular weight on the structure and crystallinity of poly (3-hexylthiophene)." Macromolecules, 2006, 39, 2162-2171.
[40]. Motaung, D.E., Malgas, G.F. and Arendse, C.J., "Correlation between the morphology and photo-physical properties of P3HT: fullerene blends." J. Mater. Sci., 2010, 45, 3276-3283.
[41]. Saini, V., Abdulrazzaq, O., Bourdo, S., Dervishi, E., Petre, A., Bairi, V.G., Mustafa, T., Schnackenberg, L., Viswanathan, T. and Biris, A.S., "Structural and optoelectronic properties of P3HT-graphene composites prepared by in situ oxidative polymerization." J. Appl. Phys., 2012, 112, 054327.
[42]. Shafiee, A., Salleh, M.M. and Yahaya, M., "Determination of HOMO and LUMO of [6, 6]-phenyl C61-butyric acid 3-ethylthiophene ester and poly (3-octyl-thiophene-2, 5-diyl) through voltametry characterization." Sains Malaysiana, 2011, 40, 173-176.
[43]. Xiao, B., Du, M., Wang, X., Xiao, Z., Li, G., Tang, A., Ding, L., Geng, Y., Sun, X. and Zhou, E., "Effects of oxygen atoms introduced at different positions of non-fullerene acceptors in the performance of organic solar cells with poly (3-hexylthiophene)." ACS appl. Mater. & interfaces, 2019, 12, 1094-1102.
[44]. Lai, T.H., Tsang, S.W., Manders, J.R., Chen, S. and So, F., "Properties of interlayer for organic photovoltaics." Mater. Tod., 2013, 16, 424-432.
[45]. Steim, R., Kogler, F.R. and Brabec, C.J., "Interface materials for organic solar cells." J. Mater. Chem., 2010, 20, 2499-2512.
[46]. Sharma, B.K., Khare, N. and Ahmad, S., "A ZnO/PEDOT: PSS based inorganic/organic hetrojunction." Solid State Commun., 2009, 149, 771-774.
[47]. Morais, T.D.D., Chaput, F., Lahlil, K. and Boilot, J.P., "Hybrid Organic–Inorganic Light-Emitting Diodes." Adv. Mater., 1999, 11, 107-112.
[48]. Ameri, T., Khoram, P., Min, J. and Brabec, C.J., "Organic ternary solar cells: a review." Adv. Mater., 2013, 25, 4245-4266.
[49]. Koster, L.J.A., Mihailetchi, V.D. and Blom, P.W., "Ultimate efficiency of polymer/fullerene bulk heterojunction solar cells." Appl. Phys. Lett., 2006, 88, 093511.
[50]. Wang, J., Yao, H., Xu, Y., Ma, L. and Hou, J., "Recent progress in reducing voltage loss in organic photovoltaic cells." Mater. Chem. Front., 2021, 5, 709-722.
[51]. Jiang, B.H., Chen, C.P., Liang, H.T., Jeng, R.J., Chien, W.C. and Yu, Y.Y., "The role of Y6 as the third component in fullerene-free ternary organic photovoltaics." Dye. Pigment., 2020, 181, 108613.

[Downloaded from nezarat.iust.ac.ir on 2025-07-18]

[DOI: 10.22068/ijmse.3147]